



A finite element modeling of drained triaxial test on loose sand using different constitutive models

N. Hasanpouri Notash¹, R. Dabiri*¹, M. Hajjalilue Bonab², L. Khodadadi³, F. Behrouz Sarand¹

¹ Department of Civil Engineering, Tabriz Branch, Islamic Azad University, Tabriz, Iran

² Department of Civil Engineering, University of Tabriz, Tabriz, Iran

³ Department of Electrical Engineering, Tabriz Branch, Islamic Azad university, Tabriz, Iran

Review History:

Received: Dec. 19, 2022

Revised: Mar. 14, 20

Accepted: May, 08, 2023

Available Online: May, 16, 2023

Keywords:

Numerical simulation

triaxial test

sand

constitutive model

Abaqus

ABSTRACT: Numerical modeling of soil can be used as a complementary or alternative method for laboratory tests. Therefore, in the simulations of geotechnical problems, properly using constitutive models (such as the cap model) requires accurate calibration of the model parameters. In the present study, the draining behavior of Nevada sand at a relative density of 40% was evaluated using Mohr-Coulomb (MC), Drucker-Prager (DP), and modified Drucker-Prager/cap (MDPC) models in Abaqus and compared with laboratory data. In this context, the conventional triaxial compression (CTC) technique was used for finite element modeling of selected drained triaxial tests by keeping the radial stress constant and increasing the axial stress. Based on the results, MC and DP constitutive models, where the behavior of the materials is linear elastic-perfectly plastic, at high confining pressures, due to the inability to simulate soil hardening, showed significant differences with the experimental results. In other words, with increasing confining pressure, the behavior of sand tends to harden, and the ability of the MDPC model, which has a hardening function based on volumetric plastic strain, increased in simulating sand behavior. Proper determination of cap parameters can have a significant effect on the results. In the present study, cap hardening parameters for Nevada sand have been determined based on experimental data.

1- Introduction

Elastoplastic models are usually used to simulate the behavior of soils. In this context, the elastoplastic laws obtained based on Terzaghi's effective stress principle are often used for analyzing the effective stress field for soil. While appropriate models for saturated solids (e.g., rocks) are properly expressed by Biot's effective stress theory (known as poroelasticity theory), which considers solid and fluid parts for geomaterials [1]. Investigating the failure mechanism and crack propagation in rocks and rock-like materials is also essential [2,3]. Generally, constitutive models can be evaluated for soil in two approaches: with and without the cap. Constitutive models without the cap are models whose yield surface in a specific confining pressure has a constant shape and are divided into two categories: pressure-independent yield surface (suitable for low friction materials such as metals) and pressure-dependent yield surface (e.g., Mohr-Coulomb and Drucker-Prager models). These constitutive models have fixed yield surfaces, and the effect of plastic deformation under hydrostatic compression is not considered. In contrast, constitutive models with the cap are models whose yield surface, in addition to changing at different hydrostatic pressure, also changes at constant hydrostatic pressure by considering the material's hardening.

Mohr-Coulomb and Drucker-Prager are two of the most popular without the cap constitutive models for soil. One of the main disadvantages of the Mohr-Coulomb criterion is the presence of corners on the yield surface. The Mohr-Coulomb yield criterion is a hexagonal pyramid in the Π plane that reasonably determines the failure locus compared to the data obtained from the experimental results. Studies showed that the actual surface of the failure is softer than the hexagon. These corners can imply singularities in the yield function [4,5]. Therefore, this causes the Mohr-Coulomb yield criterion leads to numerical difficulties when treating plastic flow at the corners of the yield surface [5,6]. In other words, in the case of using the associated flow rule, where the yield function is equal to the potential function, the Mohr-Coulomb model will encounter numerical problems in which the non-associated flow rule must be used. Researchers have proposed a softer yield surface to overcome these problems by modifying the Mohr-Coulomb model. In this context, the Drucker-Prager yield function can be used mainly to express the behavior of sand [7]. Studies have shown that using the cap model appropriately expresses sand behavior. The reason is the ability to consider the effect of stress history, stress path, dilatancy, and the effect of the intermediate principal stress [8–10]. In other words, during dynamic loading, the plastic hardening of volume is critical to sandy soils, and it is appropriate to simulate its behavior using the cap model

*Corresponding author's email: rouzbeh_dabiri@iaut.ac.ir



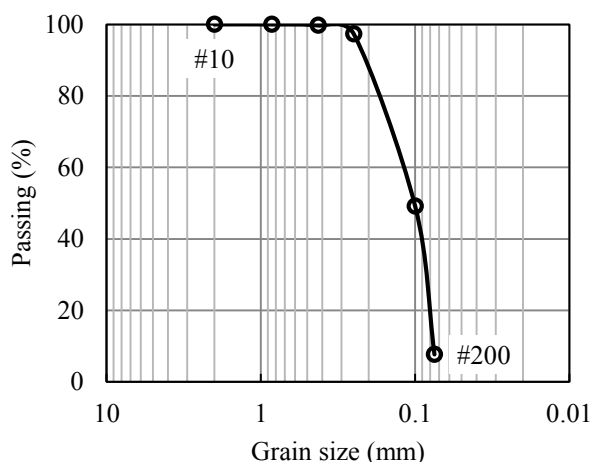


Fig. 1. Grain size distribution curve [17].

[11,12]. Therefore, if the numerical modeling of soil behavior is simulated correctly, it can be used as a complementary or alternative method for laboratory tests [13–15]. Accordingly, using advanced constitutive models (such as the cap model) to simulate geotechnical engineering problems requires accurate calibration of the input model parameters. According to Calvello and Finno (2004), inverse analysis can be used to calibrate the parameters based on reducing the difference between experimental and numerical modeling results [16]. In this way, the initial values are assumed for parameters whose values are not precisely available, and the numerical modeling results are compared with that of the experimental data. This process continues until both results are matched. In the present study, the hardening parameters of the modified Drucker-Prager/Cap (MDPC) constitutive model are presented for Nevada sand ($D_r = 40\%$) based on laboratory data and using the inverse method, which can be used in future studies for numerical simulation of this type of sand. Also, the results obtained from the Mohr-Coulomb (MC) and Drucker-Prager (DP) constitutive models are presented..

2- Materials

The soil used in the present study is Nevada sand. Nevada Sand (#120) was used during the VELACS Research Program (Verification of Liquefaction Analyses by Centrifuge Studies) by the Earth Technology Corporation in the 1990s. The results of this project, supported by the National Science Foundation (NSF), were presented by Arulmoli et al. (1992) at two relative densities of 40% and 60% [17]. Nevada sand is uniformly graded soil with an average grain size of about $D_{50} = 0.15$ mm and is quartz sand [18]. The grain size distribution curve of Nevada sand is presented in Fig. 1.

2- 1- Friction angle

The present study determined the friction angle for Nevada

sand from the consolidated drained (CD) and undrained (CU) triaxial tests from the VELACS project. The CD and CU triaxial test standards were EM1110-2-1906(X)² and D4767-88, respectively. ‘EM’ and ‘D’ are related to the Department of the US Army’s standard and ASTM standard, respectively. The drained friction angle of the soil can be calculated from the slope of the critical state line (CSL), M , in the p' - q' space by Eq. (1):

$$\phi' = \sin^{-1} \frac{3M}{6+M}, \quad M = \left(\frac{q'}{p'} \right)_{at \ failure} \quad (1)$$

Fig. 2 shows the results of 6 triaxial tests in drained and undrained conditions. Drained conditions related to the tests: (CIDC, No. 40-107), (CIDC, No. 40-100), (CIDC, No. 40-106), and the undrained conditions are related to the tests (CIUC, No. 40-06), (CIUC, No. 40-04) and (CIUC, No. 40-05), which are conducted at three effective consolidation stresses (p') of 40, 80, and 160 kPa, respectively. It should be noted that the effective consolidation stresses were constant during the CD tests ($p' = cte$). According to Fig. 2, the slope of the critical state line was determined to be about 1.34. The angle of this line relative to the p' axis indicates the parameter β (friction angle) in the Drucker-Prager model. CSL is the best line fitted to the experimental data in the p' - q' ($q = q'$) space, and its slope represents M in Eq. (1). According to this figure, the peak friction angle of Nevada sand at a relative density of 40% was obtained equal to 33° , equivalent to the friction angle of 53° in the Drucker-Prager model.

2- 2- Dilation angle

Shear resistance in sand depends on components such as interparticle friction (ϕ'_μ), particle rearrangement (critical-

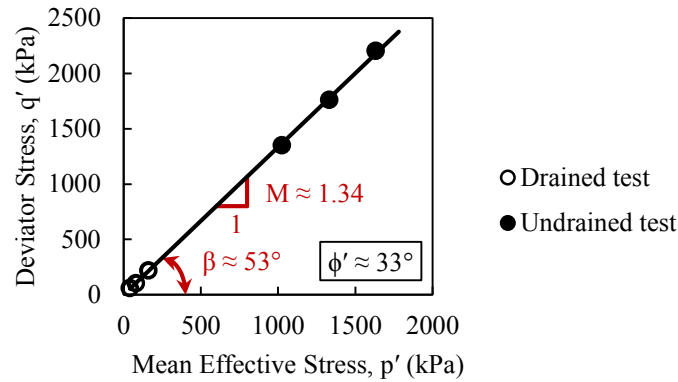


Fig. 2. Drained and undrained triaxial test results for Nevada sand at a relative density of 40% (Arulmoli et al., 1992) [17].

state shear strength), and dilatancy. The dilation angle controls the amount of plastic volumetric strain in the material during plastic shearing. For granular materials, the dilation angle can be estimated by using the well-known equation: $\psi = \phi - 30^\circ$. According to Bolton (1986) and Schanz and Vermeer (1996), the dilation angle of soil is related to the peak friction angle (ϕ'_p) and the critical friction angle ($\phi'_{cs} = \phi'_{cv}$) [19,20]. Bolton (1986) studied the resistance and dilatancy of 17 types of sands in different densities and confining pressures in axisymmetric and plane strain conditions. The dilatancy curve slope depends on the sand's relative density and the mean effective stress at failure. Thus, Bolton (1986) studied the dependence of ($\phi'_p - \phi'_{cs}$) with relative density and mean effective stress and suggested Eq. (2) based on experimental results:

$$I_R = I_D(Q - \ln p') - R_Q \quad (2)$$

Where I_R is the relative dilatancy index, I_D is the relative density of sand ($I_D = D_r/100$), p' is the mean effective stress at the peak shear strength in kPa, Q and R_Q are also fitting parameters that depend on the intrinsic properties of sand. According to Bolton (1986), $Q = 10$ and $R_Q = 1$ had the best fit with experimental results. However, based on Castro (2001) [21], the values of $Q = 9.5$ and $R_Q = 0.7$ were obtained for Nevada sand from the undrained triaxial compression test [22]. Relative density (I_D) can be calculated from $I_D = (e_{max} - e)/(e_{max} - e_{min})$, where e_{max} and e_{min} are the maximum and minimum void ratios, respectively.

According to Schanz and Vermeer (1996), the peak dilation angle ψ_p can be estimated from Eq. (3) for both triaxial strain and biaxial strain [20]:

$$\sin \psi_p = \frac{0.3I_R}{2 + 0.3I_R} \quad (3)$$

Where I_R can be determined using Eq. (2). Therefore, the dilation angle can be calculated as a function of the mean effective stress p' using the above equation.

2- 3- Shear and Young's modulus

In the present study, the maximum shear modulus of sand was considered as Eq. (4):

$$G_{max} = 8125(p')^{0.5} \quad (4)$$

Where p' and G_{max} are both in kPa. Young's modulus of the soil can be estimated from the shear modulus, as Eq. (5).

$$E_{max} = 2(1 + \nu)G_{max} \quad (5)$$

Poisson's ratio of Nevada sand was considered 0.33.

3- Constitutive models

3- 1- Mohr-Coulomb (MC) model in Abaqus

The Mohr-Coulomb yield criterion can be considered the generalized Tresca model. In both models, it is assumed that the maximum shear stress defines the yield criterion of the material. The value of the ultimate shear stress in the Tresca model is constant, while in the Mohr-Coulomb model is a

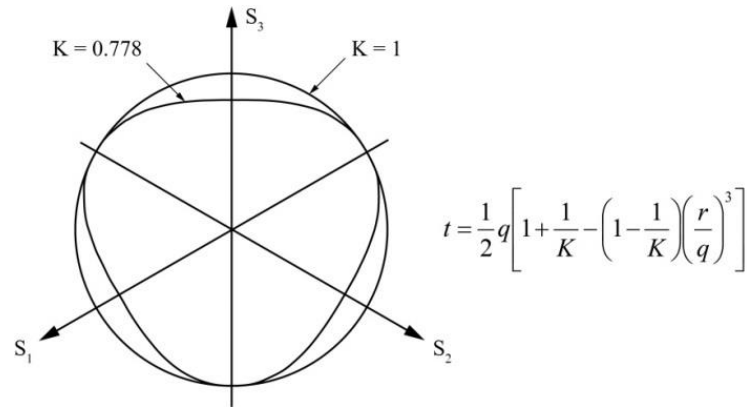


Fig. 3. Modified Drucker-Prager yield surface in the deviatoric principal stress plane (Π -plane).

function of the normal stress that acts on the specific plane. Shear strength in the Mohr-Coulomb criterion increases with increasing normal stress. The Mohr-Coulomb model implemented in Abaqus is based on the classic MC yield criterion, which includes a straight line in the meridian plane (i.e., p - t plane, where p is the hydrostatic stress and t is the deviatoric stress) and a six-sided polygon in the deviatoric plane (i.e., Π plane). In general, the plastic flow of this model in Abaqus is always non-associated. This model uses a smooth plastic flow potential instead of the classic hexagonal pyramid [23].

3- 2- Extended Drucker-Prager plasticity model (DP) in Abaqus

The extended Drucker-Prager model can be used to describe the behavior of frictional materials (such as granular soils) that exhibit pressure-dependent yield. In other words, this model is used for materials that become harder as the pressure increases. The yield surface of the DP criterion in Abaqus can be linear, hyperbolic, and exponential. A linear model with the non-associated flow rule is usually used in the p - t plane for granular materials [10]. The Drucker-Prager model implemented in Abaqus is defined as Eq. (6):

$$f = t - p \tan \beta - d = 0 \tag{6}$$

Where β is the friction angle (the slope of the shear yield surface in the p - t plane), and d is the cohesion. Also, p is the hydrostatic stress obtained from Eq. (7).

$$p = -\frac{1}{3} \text{trace}(\boldsymbol{\sigma}) \tag{7}$$

In Eq. (6), t is the deviatoric stress and is given by:

$$t = \frac{1}{2} q \left[1 + \frac{1}{K} - \left(1 - \frac{1}{K} \right) \left(\frac{r}{q} \right)^3 \right] \tag{8}$$

Where q is the Mises equivalent stress, r is the third invariant of deviatoric stress, and K is the flow stress ratio, which indicates the yield stress ratio in triaxial tension to yield stress in triaxial compression and is a scalar parameter. The flow stress ratio determines the shape of the yield surface, which according to Fig. 3, controls the curvature of the yield surface in the deviatoric principal stress plane (Π -plane). The maximum value of K is equal to 1, in which case the shape of the yield surface will be a circle, and the third stress invariant will not affect the yield surface. According to Eq. (8), if $K = 1$, then $t = q$. By reducing K , the shape of the yield surface will be triangular with smoothly rounded edges, as shown in Fig. 3. Therefore, it is possible to define non-circular yield surfaces in the Π -plane by reducing the K value. Based on the principles of plasticity, the yield surface must be convex. To ensure the yield surface's convexity, the K value cannot be less than 0.778 (i.e., $0.778 \leq K \leq 1.0$). It should be noted that in the plane strain condition, the value of this parameter is considered equal to 1, but in the triaxial condition can be determined from Eq. (9) [10]. According to Helwany (2007), the setting of $K = 1$ has properly simulated the triaxial stress-strain response of Ottawa sand ($\phi = 37^\circ$) at two confining stresses of 35 and 70 kPa [9].

$$K = \frac{3 - \sin \phi}{3 + \sin \phi}, \quad (0.778 \leq K \leq 1) \tag{9}$$

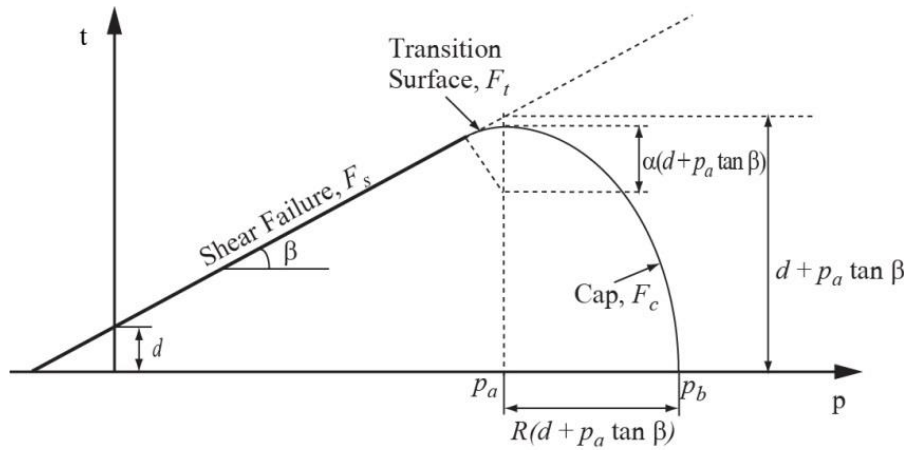


Fig. 4. Yield surface of the MDPC model in the p-t plane [9].

3- 3- Modified Drucker-Prager/Cap (MDPC) plasticity model in Abaqus

The cap model implemented in the Abaqus defines the transfer surface to the Drucker-Prager cap model. This additional yield surface located between the shear failure surface and the cap surface is known as the modified Drucker-Prager/cap (MDPC) model in the literature. This constitutive model can simulate materials whose compressive yield strength is more significant than tensile yield strength (such as rock and soil). As shown in Fig. 4, the yield surface of the MDPC implemented in Abaqus includes three parts: the Drucker-Prager shear failure surface, an elliptical cap intersecting the mean effective stress axis, and a smooth transition between the shear failure and the cap surface. The smooth transition region is introduced to achieve convergence in the numerical analysis [24,25]. The Drucker-Prager failure part is a perfectly plastic yield surface (without hardening). Plastic flow in the Drucker-Prager shear failure surface produces a volumetric plastic dilation, causing the cap to soften. While the plastic flow on the cap surface causes the material to compaction [10]. In other words, when the stress conditions cause yielding on the cap, volumetric plastic strains cause hardening, and as a result, the cap becomes larger. On the other hand, if the stress conditions led to yielding on the Drucker-Prager shear failure surface, volumetric plastic dilation caused the cap to shrink (softening) [9]. According to Fig. 4, because at the point of intersection of the cap with the p-axis, the induced strains are only volumetric type, the cap intersects the mean effective stress axis at a right angle. In the cap region, flow potential is similar to the yield surface (i.e., flow is associated). While for the Drucker-Prager shear failure surface and the transition yield surface, the flow is

non-associated.

As shown in Fig. 4, the cap yield surface is an ellipse with an eccentricity of R in the p-t space, which depends on the third stress invariant, r, in the deviatoric plane (See Fig. 3). The cap yield surface as a function of volumetric plastic strain hardens (expands) or softens (shrinks), which is expressed as Eq. (10):

$$F_c = \sqrt{(p - p_a)^2 + \left(\frac{Rt}{1 + \alpha - \frac{\alpha}{\cos \beta}} \right)^2} - R(d + p_a \tan \beta) = 0 \quad (10)$$

Where R is the material parameter that, according to Fig. 4, controls the cap shape. This parameter must be greater than zero and can be determined based on the contours of constant plastic volumetric strains from experimental results (conventional triaxial compression test and hydrostatic compression test) [26,27]. Based on Han et al. (2008), values of R range from 0.0001 to 1000 [28]. Desai and Siriwardane (1984) reported R values in the range of 1.67 to 2 (for artificial soil). However, this parameter for Ottawa sand has been considered 0.4 [9] and 2.45 in dense conditions [11]. Similar to Lee et al. (2010), R can be determined by the inverse method using numerical simulations [12]. The value of this parameter depends on the mean stress, p. As the mean stress increases, R decreases. Lee et al. (2010) obtained R values from the inverse method for Tsukuba sand using LS-DYNA finite element software, ranging between 5 and 8 under mean stresses of 100 and 40 kPa, respectively.

In Eq. (10), α is a small number (usually 0.01 to 0.05)

utilized to define a smooth transition surface between the Drucker-Prager shear failure surface and the cap. If this parameter is considered zero ($\alpha = 0$), the MDPC model does not have a transition region, implying a sharp-edge connection between the shear failure and the cap surfaces [29]. The lack of a transition region can lead to convergence problems. Therefore, if it is assumed that the transition zone does not exist in this model, it is better to use small values for α (for example, 0.001) [30]. This parameter is usually between 0.01 and 0.05, which for Ottawa sand has been considered 0.05 [9] and 0.01 [11] in the literature. The transition surface in the MDPC model is defined as Eq. (11):

$$F_t = \sqrt{(p - p_a)^2 + \left[t - \left(1 - \frac{\alpha}{\cos \beta} \right) (d + p_a \tan \beta) \right]^2} - \alpha(d + p_a \tan \beta) = 0 \quad (11)$$

As mentioned before, $K = 1$ causes the deviatoric stress (t) will be equal to the Mises equivalent stress (i.e., $t = q$). Therefore, in the triaxial test, it will be $t = q = \sigma_1 - \sigma_3$, where σ_1 and σ_3 are the maximum and minimum principal stresses, respectively [10].

In Eqs. (10) and (11), p_a is a parameter that controls the hardening-softening behavior as a function of the plastic volumetric strain, which is also called the evolution parameter and is defined as:

$$p_a = \frac{p_b - Rd}{(1 + R \tan \beta)} \quad (12)$$

Where p_b is the hydrostatic compression yield stress that, according to Eq. (13), is defined as a function of volumetric plastic strain.

$$p_b = p_b(\varepsilon_{v0}^p + \varepsilon_v^p) \quad (13)$$

Where ε_{v0}^p shows the initial condition of the material at the beginning of the analysis. Hardening-softening behavior can be defined by a piecewise linear function relating the mean effective stress p_b and the volumetric plastic strain. This curve can be determined from an isotropic consolidation test with several unloading-reloading cycles [9]. The slope of the unloading-reloading line can be used to calculate the volumetric elastic strain. The contribution of elastic strain must be subtracted from the total volumetric strain to calculate volumetric plastic strain. In saturated soft soils, no volume change might occur during seismic loading caused by assuming undrained conditions. In these cases, the Drucker-Prager model should be used instead of the MDPC model (without considering the volumetric plastic hardening) [11].

4- Volumetric strain under hydrostatic loading for Nevada sand

In the MDPC constitutive model, the volumetric strain that occurs under hydrostatic loading can be determined based on experimental data from Lade and Abelev (2005) for Nevada sand. As is known, the stress history of soil (maximum effective stress that the soil has endured in its geological history) plays an essential role in the behavior of granular soil [31–33]. Therefore, comprehensive experimental data for the hydrostatic compression of Nevada sand will be required to consider the effect of the initial position of the hardening cap (p'_0) on soil resistance and the determination of strain components at different stress levels. The models presented in the literature for the hydrostatic compression of Nevada sand were used in the present study to determine the volumetric plastic strains at the relative density of 40% under different confining stresses. Table 1 summarizes these hydrostatic compression models to estimate the volumetric strain of sand.

Fig. 5 shows the hydrostatic compression curves obtained from models listed in Table 1 and the results of the Lade and Abelev (2005) tests for Nevada sand at two relative densities of 30% and 70%. As can be seen from this figure, Vallejos (2008) [37] and Lee et al. (2010) [12] models have shown the best agreement with the experimental results. The volumetric strain calculated by Qubain et al. (2003) [35] and Lee et al. (2010) were obtained almost the same.

In Fig. 5, ε_v represents the total volumetric strain. Total volumetric strain is the sum of the elastic strain increment and plastic strain increment. Therefore, the total volumetric strain calculated from the proposed models, as presented in Table 1, must be subtracted from the elastic strain to determine the plastic volumetric strain. The increment of elastic volumetric strain during hydrostatic loading can be determined from Eq. (14):

$$\delta \varepsilon_v^e = \frac{\delta p'}{K'} = \kappa \frac{\delta p'}{v p'} \quad (14)$$

Where $\delta \varepsilon_v^e$ is elastic volumetric strain increment, $\delta p'$ denotes hydrostatic pressure increment, K' is the bulk modulus, κ is the slope of the unloading-reloading line in the e - $\ln(p')$ space, v represents the specific volume of soil ($v = 1+e$) at the starting of loading (i.e., $e = e_0$), and p' is the hydrostatic pressure at the starting of loading ($p' = p'_0$). According to Eq. (14), bulk modulus refers to the ratio of hydrostatic stress to volumetric strain change. Therefore, tangent bulk modulus can be determined by differentiating equations in Table 1 concerning the hydrostatic stress p' . The tangent bulk modulus is the slope of the stress-strain curve at any given stress or strain. Therefore, the amount of plastic volumetric strain can be determined as [12]:

Table 1. Proposed models to predict the volumetric strain of sandy soils under hydrostatic loading.

| Model No. | formula and description | Parameter values for Nevada sand | Reference |
|-----------|--|---|---------------------------------|
| 1 | $\varepsilon_v = \frac{e_0}{1+e_0} \left\{ 1 - \exp \left[-\beta e_0^{\frac{1}{\rho_c}} \left(\frac{p'}{p_{atm}} \right) \right] \times \exp \left[-\frac{3}{2C_b} \left(\frac{p'}{p_{atm}} \right)^{\frac{2}{3}} \right] \right\}$ <p>e_0: initial void ratio of sand, β: dimensionless parameter, ρ_c: compression coefficient in the limiting compression curve (LCC), C_b: dimensionless elastic coefficient, p': hydrostatic pressure, p_{atm}: atmospheric pressure (100 kPa)</p> | $\rho_c^* = 0.365$ $\beta = 0.0023$ $C_b = 850$ | Pestana and Whittle (1995) [34] |
| 2 | $\varepsilon_v = \frac{bp'}{1+mp'}$ <p>b and m: intercept and the slope of straight-line isotropic compression for sandy soil, in the volumetric strain versus the ratio of volumetric strain to effective mean stress space (i.e., $\varepsilon_v - \varepsilon_v/p'$), respectively.</p> | $D_r = 30\%$: $b^{**} = 0.0039$ $m^{**} = 0.001$ $D_r = 70\%$: $b^{**} = 0.0026$ $m^{**} = 0.0009$ | Qubain et al. (2003) [35] |
| 3 | $\varepsilon_v = \frac{2(1.5 - D_{r0})}{C} \sqrt{\frac{p'}{p_{atm}}}$ <p>D_{r0}: initial relative density, C: material constant, p_{atm}: atmospheric pressure (100 kPa)</p> | $C = 220$ | Park and Byrne (2004) [36] |
| 4 | $\varepsilon_v = \frac{1}{1+e_0} \left\{ \left[\frac{p_{atm}}{A_s} \left(\frac{1+e_0}{b-e_0} \right)^2 \right] \frac{1}{\alpha_v} \left(\frac{p'}{p_{atm}} \right)^{\alpha_v} \right\}$ <p>e_0: initial void ratio, p_{atm}: atmospheric pressure (100 kPa), p': hydrostatic pressure, A_s, b, and α_v parameters used for sandy soils</p> | $A_s/p_{atm}^\dagger = 637$ $b = 1.571$ $\alpha_v = 0.37$ | Vallejos (2008) [37] |
| 5 | $\varepsilon_v = \frac{p'}{K_i + \frac{1}{(\varepsilon_v)_{asy}} p'}$ <p>p': hydrostatic pressure, K_i: initial tangential bulk modulus, and $(\varepsilon_v)_{asy}$: asymptotic total volumetric strain that occurs at $p' = \infty$</p> | $D_r = 30\%$: $K_i^{\ddagger} = 26000$ $(\varepsilon_v)_{asy}^{\ddagger} = 4.1$ $D_r = 70\%$: $K_i^{\ddagger} = 38783$ $(\varepsilon_v)_{asy}^{\ddagger} = 2.95$ | Lee et al. (2010) [12] |

* Average values of Manchester fine sand and Toyoura sand

** Units: b (%/kPa), m (1/kPa)

† Specimen preparation technique (Air Pluviation, AP)

‡ Units: K_i (kPa), $(\varepsilon_v)_{asy}$ (%)

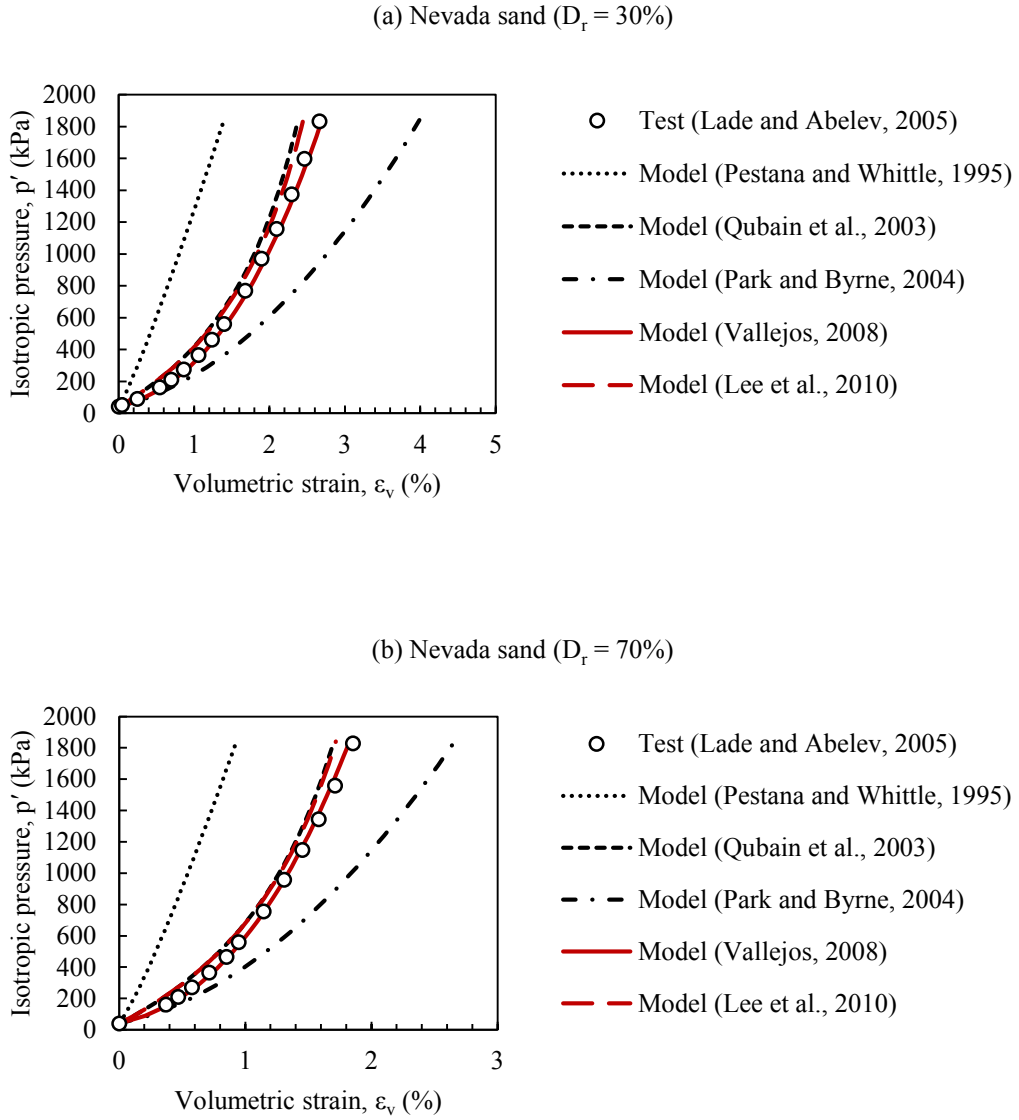


Fig. 5. Measured (prepared by Air Pluviation method) and predicted values for hydrostatic compression of Nevada sand (a) $D_r = 30\%$, and (b) $D_r = 70\%$.

$$\varepsilon^p = \varepsilon_v - \frac{p'}{K_t} \quad (15)$$

$$\varepsilon_v^p = \frac{\lambda - \kappa}{1 + e_0} \ln \frac{p'}{p'_0} \quad (16)$$

Where p' is the hydrostatic stress at each loading step and K_t is the tangential bulk modulus.

In addition to the models presented in Table 1, the soil plastic volumetric strain can be directly calculated from the Cam clay model using Eq. (16) [9,38].

Where λ and κ are material parameters. λ and κ for Nevada sand can be determined from the hydrostatic compression curves reported by Vallejos (2008) based on the experimental data of Lade and Abelev (2005). In the present study, λ and κ for Nevada sand at the relative density of 40% were

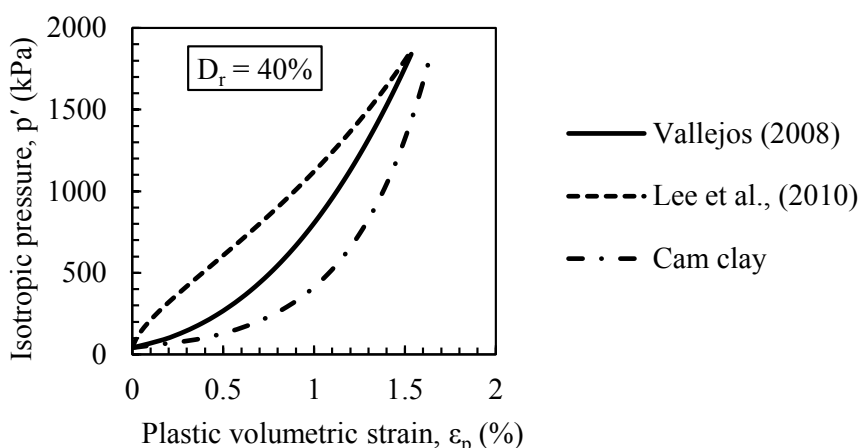


Fig. 6. The volumetric plastic strain of Nevada sand at a relative density of 40%.

considered equal to 0.012 and 0.0045, respectively.

Fig. 6 shows the volumetric plastic strain of Nevada sand for the initial confining stress (p'_0) of 40 kPa. As can be seen, the Cam clay model overestimated the volumetric plastic strain. Also, the calculated values of elastic strain up to hydrostatic stress of about 1050 kPa have been greater than those of plastic strain in the Lee et al. (2010) model. However, the elastic strain amplitude is a small fraction of the total strain [34]. Based on this, it seems that the Lee et al. (2010) model cannot correctly predict the plastic strains which develop in the Nevada sand. Therefore, the present study used the Vallejos model to determine the cap parameters.

5- Calibration of resistance parameters for triaxial condition

5- 1- Friction angle

To determine the Drucker-Prager parameters (β and d), it is necessary to have the results of at least three triaxial compression tests. The at-failure conditions obtained from the results of the tests can be plotted in the p - t plane. A straight line is then fitted to these points. The intersection of this line with the t -axis represents d (cohesion in Drucker-Prager), and the slope of the line is also equal to β (friction angle in Drucker-Prager), which was previously presented in Fig. 2 for Nevada sand. In addition, Drucker-Prager model parameters (β and d) can also be determined for triaxial conditions using Mohr-Coulomb model parameters (ϕ and c) from Eqs. (17) and (18) [10]:

$$\tan \beta = \frac{6 \sin \phi}{3 - \sin \phi} \quad (17)$$

$$d = c \frac{6 \cos \phi}{3 - \sin \phi} \quad (18)$$

Where ϕ and c are the friction angle and cohesion in the Mohr-Coulomb model, respectively.

5- 2- Soil dilation

In addition to the friction angle and cohesion, the dilation angle of soil should also be calculated in the p - t space for the triaxial condition using Eq. (19) [39,40].

$$\tan \psi_{DP} = \frac{6 \sin \psi_{MC}}{3 - \sin \psi_{MC}} \quad (19)$$

Where ψ_{MC} and ψ_{DP} are the dilation angles in the σ - τ and p - t coordinate space, respectively.

5- 3- Determination of R parameter in p-t space

According to Fig. 7, two approaches were used in the present study to determine the R parameter: theory and numerical modeling (inverse method). This parameter can be obtained for Nevada sand from the triaxial compression test conducted by Arulmoli et al. (1992), according to the loading path shown in Fig. 8. In this figure, based on the drain testing procedure ($p' = cte$), the evolution parameter (p_a) is equivalent to the effective consolidation stress.

Decreasing the value of R causes the specimen to reach its maximum deviatoric stress at a faster rise. However, reducing R will no longer affect the maximum deviatoric stress when

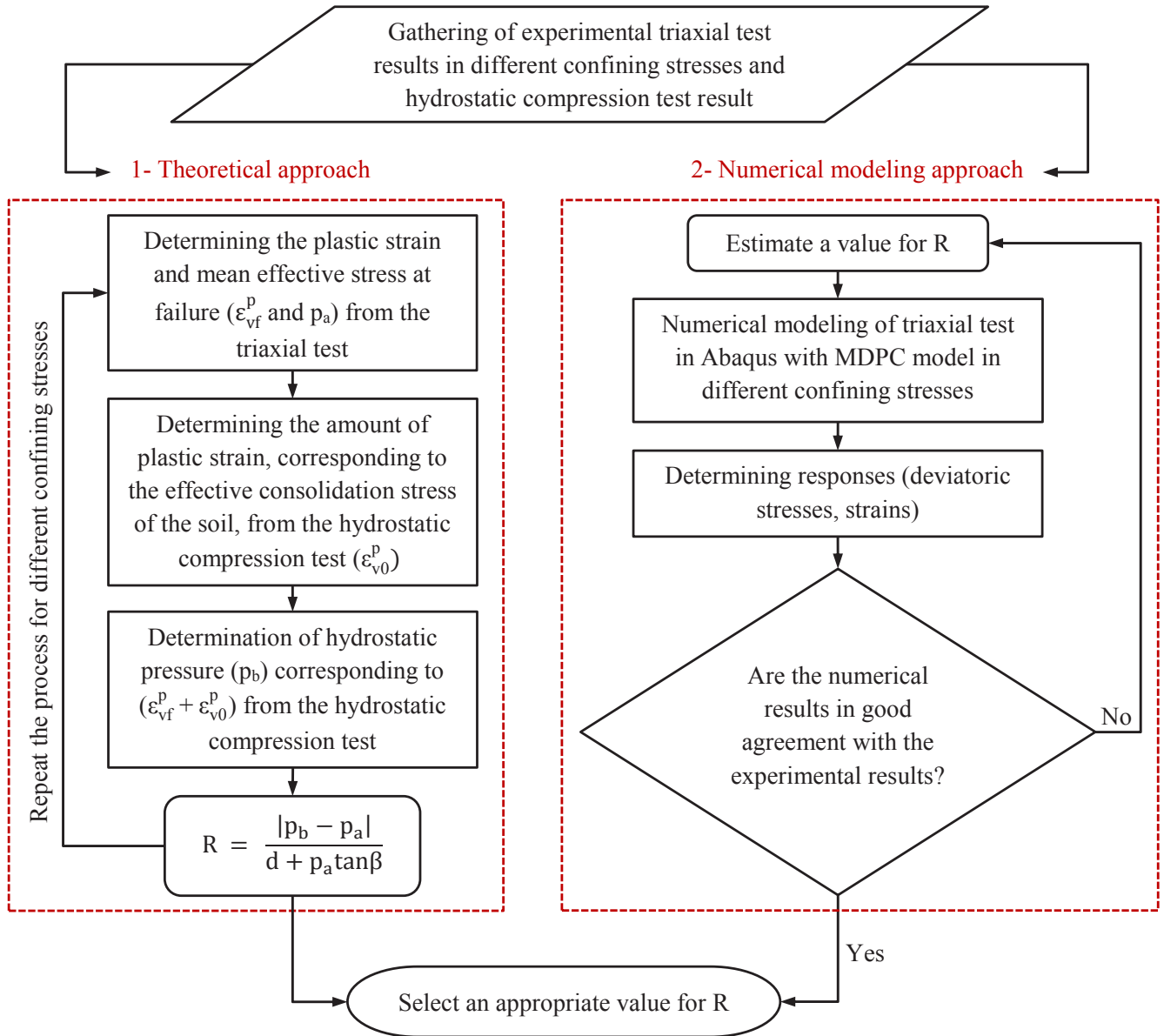


Fig. 7. Procedures for determining the R parameter in the present study.

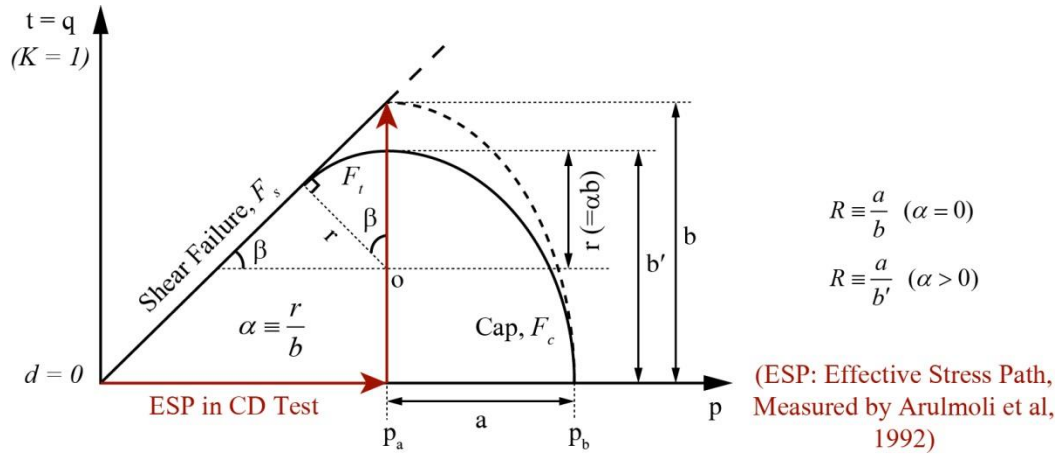


Fig. 8. The stress path in the drained triaxial test of Arulmoli et al. (1992) and the yield surfaces of the MDPC model in the p-t space to determine the R parameter ($\alpha = 0$).

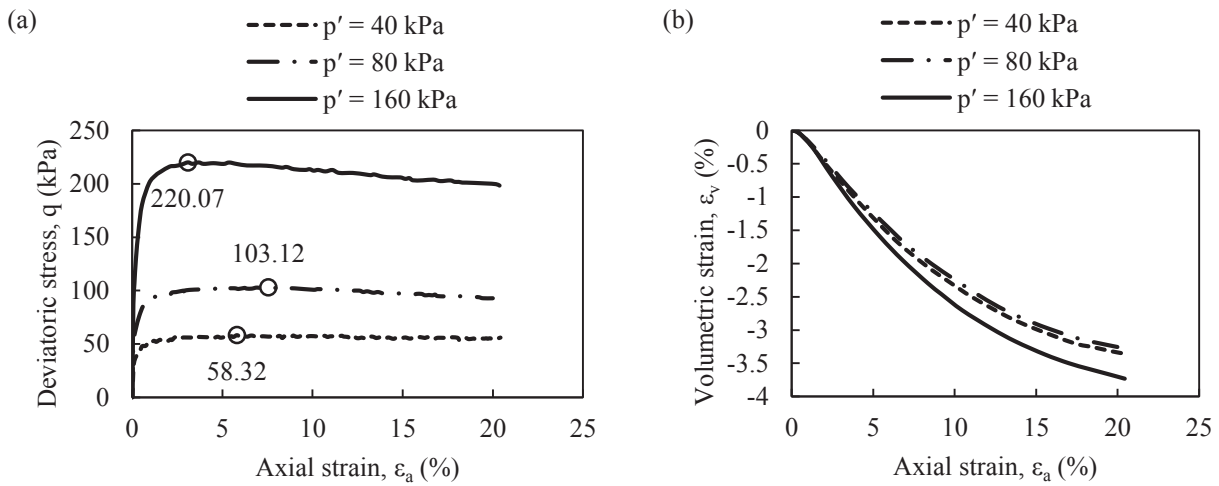


Fig. 9. CD tests results for Nevada sand at a relative density of 40% under effective consolidation stresses of 40, 80, and 160 kPa (a) $\epsilon_a - q$ diagram and (b) $\epsilon_a - \epsilon_v$ diagram (Arulmoli et al., 1992).

the soil strain reaches the ultimate value. In this condition, the maximum deviator stress of soil will be affected by the α value. In this case, increasing the α value decreases the ultimate deviatoric stress of the soil. According to Shin and Kim (2015), it is desirable to determine R by considering α as zero. In the MDPC model, α is defined only for numerical stability; therefore, it is not a material constant [25]. By setting $\alpha = 0$, R in p-t space is determined as below:

$$R = \frac{|p_b - p_a|}{d + p_a \tan \beta} \quad (20)$$

Fig. 9 shows the results of the drained triaxial tests of Nevada sand. In this figure, the peak deviatoric stresses have been shown for different effective consolidation stresses.

Table 2 shows the determination of the R parameter based on the final cap using the theoretical approach (in the p-t space). As mentioned, it is proper to obtain the R-value by setting $\alpha = 0$. Therefore, the peak shear stress measured by Arulmoli et al. (1992) was considered a failure value (See Fig. 8). Also, p_b was determined based on the Vallejos model from Eq. (21).

Table 2. Initial estimation of R parameter from the theoretical approach.

| Arulmoli et al (1992) [17] | | | Vallejos (2008) [37] | | p _a (kPa) | R [‡] |
|----------------------------|---------|---------------------------------|----------------------------------|-----------------------------------|----------------------|----------------|
| p' (kPa) | q (kPa) | ε _v (%) [*] | ε _{v0} ^p (%) | p _b (kPa) [†] | | |
| 40 | 58.32 | -1.51 | 0.49 | 82.47 | 40 | 0.8 |
| 80 | 103.12 | -1.81 | 0.64 | 121.70 | 80 | 0.39 |
| 160 | 220.1 | -0.89 | 0.82 | 0.06 | 160 | 0.75 |

* Volumetric strain corresponding to peak shear strength (q) was chosen for ε_v. In the drained triaxial test conducted by Arulmoli et al. (1992) the mean effective stress was kept constant throughout the test (No. 40-107, No. 40-100, and No. 40-106), so: (ε_e = 0) and (ε_v = ε_v^p). Also, compressive stresses and strains were considered positive in these tests.

† Calculated from Eq. (21) with e₀ = 0.748, ε_v^p = ε_v, A_s/p_{atm} = 637, b = 1.571, α_v = 0.37 and p_{atm} = 100kPa

‡ Calculated from Eq. (20) with d = 0 and β = 53°

$$p_b = \left[|\varepsilon_{v0}^p + \varepsilon_v^p| (1 + e_0) \frac{A_s}{p_{atm}} \left(\frac{b - e_0}{1 + e_0} \right)^2 \alpha_v \cdot p_{atm}^{\alpha_v} \right]^{\frac{1}{\alpha_v}} \quad (21)$$

According to Table 2, R was calculated based on volumetric strain corresponding to peak shear strength, which led to a good agreement between the theoretical approach and numerical modeling (inverse method). Based on this, ε_v for p' = 160 kPa was lower than the other tests (See Table 2). Therefore, by decreasing the volumetric plastic strain, p_b decreased according to Eq. (21), and the result of the expression |p_b - p_a| for p' = 160 kPa was obtained more than that of p' = 80 kPa. Thus, with increasing confining stress from 80 to 160 kPa due to the increase in |p_b - p_a|, according to Eq. (20), R has raised to 0.75. While compared to the value calculated for p' = 40 kPa, R has decreased with increasing mean effective stress, similar to Lee et al. (2010) study.

In the present study, according to the procedure shown in Fig. 7, the constant value of R = 0.8 was set for Nevada sand at all confining stresses. Helwany (2007) also used a constant value of 0.4 for Ottawa sand based on triaxial test results (under confining stresses of 35-70 kPa). The transition surface parameter (α) was assumed to be 0.05, previously considered for Ottawa sand in the literature [9].

6- Numerical modeling of triaxial test

In this section, the numerical simulation of the drained triaxial test has been evaluated using MC, DP, and MDPC constitutive models in Abaqus version 6.14 [41]. Also, the accuracy of the cap parameters discussed in the previous

sections for Nevada sand was investigated. The results of numerical simulations were compared with the laboratory data of Arulmoli et al. (1992) and Castro (2001). It should be noted that tests No (CIDC, 40-107), (CIDC, 40-100), and (CIDC, 40-106) from Arulmoli et al. (1992) were selected, which related to effective consolidation stresses (p') of 40, 80, and 160 kPa, respectively. The standard used in these tests was EM1110-2-1906(X)², and the diameter and height of the cylindrical specimen were 6.35 cm (2.5 inches) and 15.3 cm, respectively. Fig. 10 shows the boundary conditions of the finite element model used in the triaxial test simulation of Nevada sand in Abaqus. In this figure, O is the center of the soil specimen, and the results of the simulations (stresses and strains) have been obtained from this point.

As shown in Fig. 10, a two-dimensional axisymmetric mesh with only one element was used for soil. The chosen element was a pore fluid/stress eight-node axisymmetric quadrilateral element and reduced integration (CAX8RP). As can be seen, the vertical displacement is fixed on the lower part of the model (u_y = 0). Also, the left side of the mesh is a symmetry line (u_x = 0). On the top surface of the mesh, a uniform downward displacement was applied very slowly (strain-control triaxial test), which is a common approach in numerical simulation [9,42]. The top surface of the mesh was considered a pervious boundary during the loading. Therefore, the top and bottom of the soil specimen were allowed to drain due to the symmetry concerning the plane passing through the mid-height of the soil. The analyses were carried out in two steps: a consolidation step and a shearing step. In the first step, confining pressure was applied to the upper and right sides of the mesh. The geostatic command

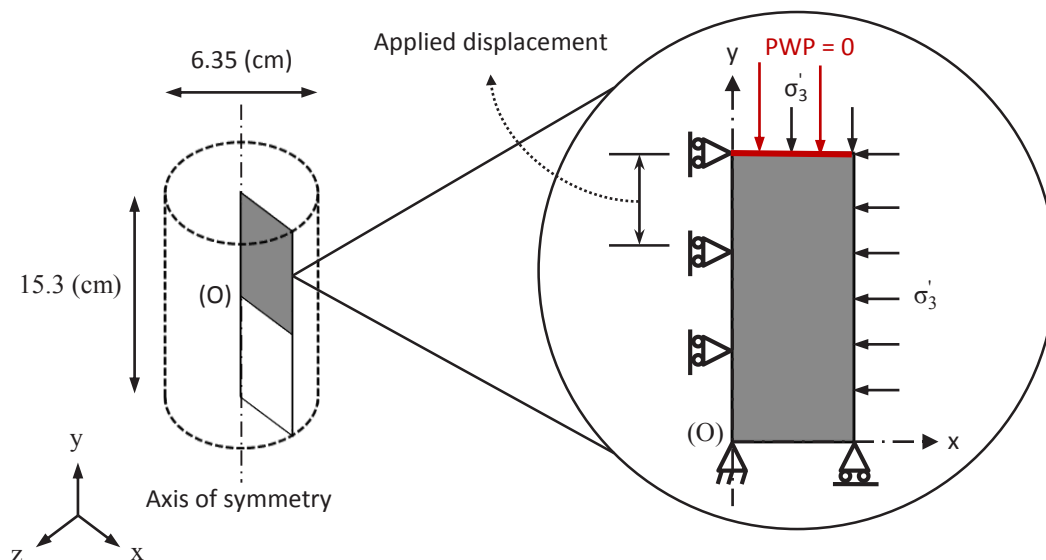


Fig. 10. Axisymmetric finite element model of the drained triaxial test used in Abaqus.

was used in this step to ensure equilibrium existence within the soil specimen. Also, to ensure that the initial horizontal stresses are the same as the vertical stresses in the first step of the test, the value of the lateral coefficient was defined as 1. The second step (shearing) was also performed (within 10^9 seconds) by applying downward displacement at a minimal rate. In this step, a displacement-type load of 1.5 cm was applied to the top surface, which type of load variation with time was considered as “ramp linearly overstep”. It should be noted that the loading rate used in the numerical simulation of the CD test should be selected so that the excess pore water pressure within the soil specimen is always zero. However, the maximum pore water pressure change was set to 7×10^{-3} kPa per time increment. This procedure is suitable for loading steps with a very long duration [9]

As mentioned before, the mean effective stress p' was constant within the soil specimen throughout the drained triaxial test of Arulmoli et al. (1992). This type of triaxial test can be simulated by changing pore water pressure (such as the periodic opening and closing of the drain tap connected to the specimen in the study of Eslami et al., 2018 [43]) using subroutine coding in Abaqus. However, to avoid numerical complexity in the present study, the drained triaxial tests of Arulmoli et al. (1992) were modeled as the conventional triaxial compression, CTC, test (keeping the radial stress constant and increasing the axial stress). Also, once again conventional drained triaxial compression test of Castro (2001), as reported by Kulasingam et al. (2004) and Jaeger et al. (2014) [44,45] a range of initial relative densities (DR), was simulated.

The model parameters for the Nevada sand are presented in Table 3. The initial position of the cap in the MDPC constitutive model, which shows the initial consolidation of the soil, was taken as $\varepsilon_{v0}^p = 0$, corresponding to the effective consolidation stresses of p' (i.e., 40, 80, 160, and 390 kPa). Also, the hydrostatic compression curves used in the cap model under consolidation stresses of 40, 80, and 160 kPa (for Arulmoli et al., 1992) and 390 kPa (for Castro, 2001) are presented in Fig. 11. Notably, a small cohesion value was used for Nevada sand in Abaqus.

7- Numerical Modeling Results

Fig. 12 shows pore water pressure and vertical displacement of the soil specimen contours obtained from the numerical simulation of the Castro (2001) test at the end of the analysis for the MDPC model. As can be seen, the pore water pressure in the center of the soil specimen is zero, so the duration of the shearing step (10^9 seconds) was a good choice and did not need to increase. Similar results were obtained for other analyses.

Fig. 13 shows the results of simulations in terms of stress paths and deviatoric stress values using Mohr-Coulomb (MC), Drucker-Prager (DP), and modified Drucker-Prager/cap (MDPC) constitutive models. In this figure, the laboratory data of Arulmoli et al. (1992) (with constant mean effective stress) and Castro (2001) (CTC test) are also presented. As mentioned, the drained triaxial tests of Arulmoli et al. (1992), similar to Castro (2001), were simulated as the CTC test in Abaqus. Fig. 13 (a) shows the measured and computed effective stress paths. In this figure, the peak stress points

Table 3. Mohr-Coulomb (MC), Drucker-Prager (DP), and modified Drucker-Prager/cap (MDPC) model parameters for Nevada sand used in the numerical simulation of the triaxial test.

| Parameter | Unit | Constitutive model | Dr = 20% | | Dr = 40% | | |
|---------------------------|-------------------|--------------------|------------------------|------------|----------------------|------------------------|-----------|
| | | | Confining stress (kPa) | | | | |
| | | | p' = 390 | p' = 40 | p' = 80 | p' = 160 | |
| ρ | kg/m ³ | In all models | 1467 | | 1523 | | |
| e_0 | - | | 0.815 | | 0.748 | | |
| k | m/sec | | | | 6.6×10^{-5} | | |
| γ_w | kN/m ³ | | | | 9.81 | | |
| G_{max} | MPa | | 160.46 | 51.39 | 72.67 | 102.77 | |
| E | MPa | | 426.81 | 136.69 | 193.31 | 273.38 | |
| ν | - | | | | 0.33 | | |
| ϕ, β^* | deg (°) | | MC DP, MDPC | | | 33 53 | |
| ψ | deg (°) | | MC DP | 0.1 0.2 | 9.9 20 | 8.2 16.7 | 6.4 13 |
| c, d^* | kPa | | MC DP, MDPC | | | 10^{-5} 10^{-5} | |
| K | - | DP, MDPC | | | 1 | | |
| $\epsilon_{v0}^p \dagger$ | - | MDPC | | | 0 | | |
| R^{\ddagger} | - | MDPC | | | 0.8 | | |
| α | - | MDPC | | | 0.05 | | |
| Cap hardening | - | MDPC | | | According to Fig. 11 | | |

* In the Drucker-Prager and cap Model (β, d) and in the Mohr-Coulomb Model (ϕ, c)

† Expresses the initial position of the cap

‡ Cap eccentricity

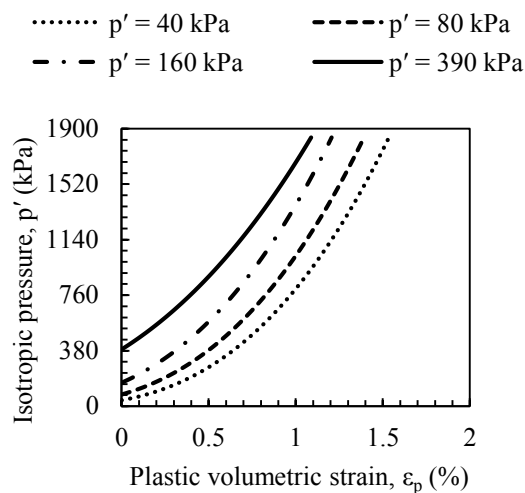
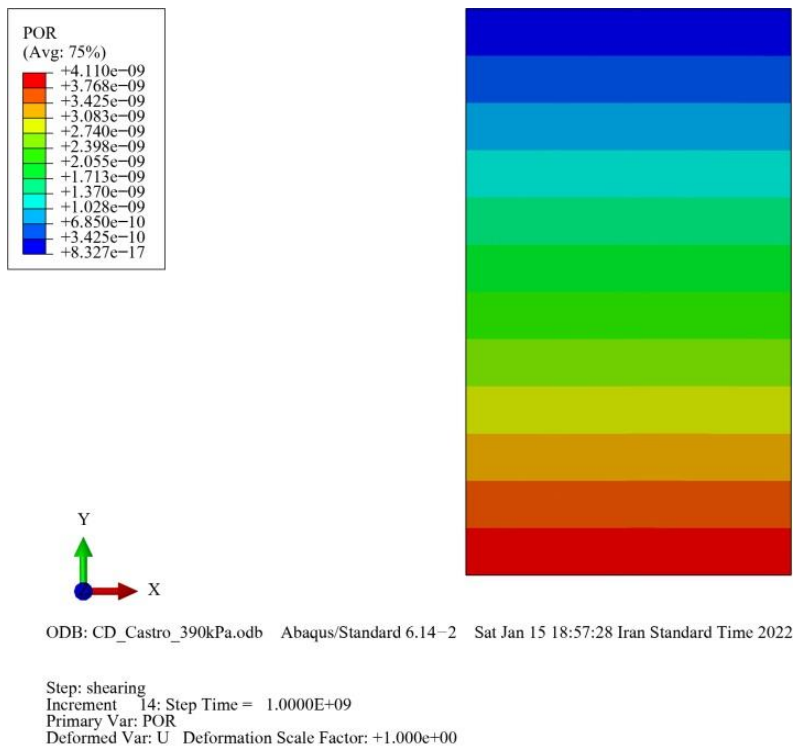
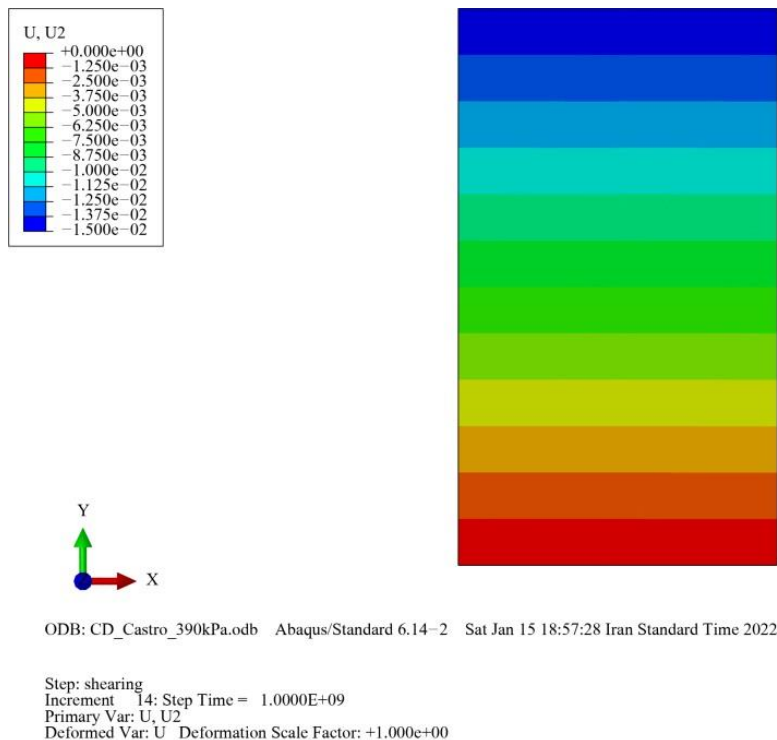


Fig. 11. Hydrostatic compression curves for Nevada sand under different effective consolidation stress based on the Vallejos (2008) model, ($A_s/p_{atm} = 637, b = 1.571, \alpha_v = 0.37$).



(a)



(b)

Fig. 12. Results of numerical simulation of Castro triaxial test using the MDPC model at the end of the analysis (a) pore water pressure contours in Pa, and (b) axial displacement contours in meter.

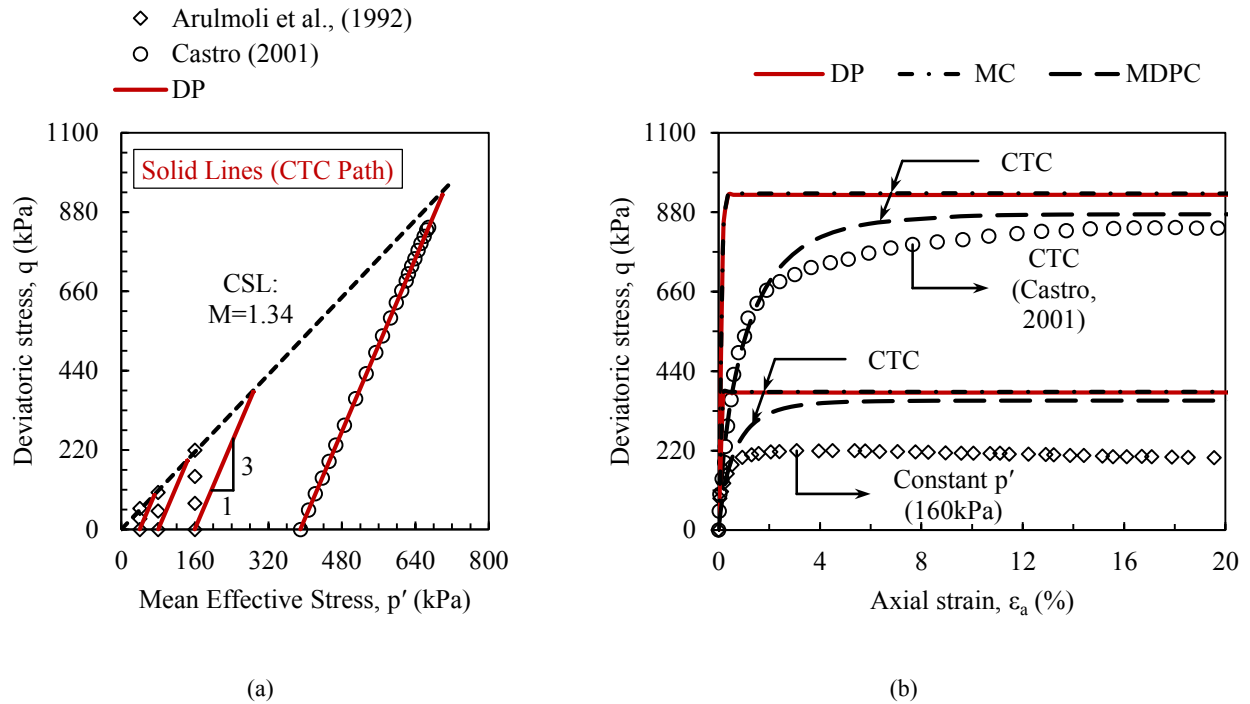


Fig. 13. Comparison of simulation results of conventional triaxial compression test (CTC) with experimental results, (a) stress paths, and (b) (ϵ_a - q) curves.

of each path represent the ultimate (failure) values. In the present study, the friction angle and slope of the critical state line, CSL (i.e., $M = q'/p'$), for Nevada sand were determined based on the triaxial test results of Arulmoli et al. (1992). However, based on the experimental data of Castro (2001), the slope of the CSL was calculated at about $M = 1.25$, and the corresponding friction angle was obtained at about 31° by the well-known equation: $\sin\phi = 3M/(6+M)$. Nevertheless, the friction angle of Nevada sand was considered $\phi = 33^\circ$ (See Table 3). For this reason, the experimental stress path of Castro (2001) has not intersected the critical state line. As can be seen, the computed effective stress path is consistent with the experimental data of Castro (2001). Also, the computed effective stress paths for Arulmoli et al. (1992) have a slope of 3:1, which resulted from the simulation of these tests as conventional triaxial compression in Abaqus. The stress paths for all constitutive models had almost similar results, and only the stress paths obtained from the DP model have been presented in Fig. 13 (a). According to Fig. 13 (b), the ultimate deviatoric stress obtained from the MC and DP constitutive models are almost the same, which indicates the appropriate matching of the resistance parameters of these two models for the triaxial condition (See section 05). As seen from this figure, in all confining stresses, maximum deviatoric stresses from the elastic-perfectly plastic models (i.e., MC and DP) were obtained about 6% more than those of the cap model (i.e., MDPC). The maximum deviatoric stresses obtained from the MC and DP constitutive models had an error of

about 11% compared with that measured by Castro (2001). However, this error for the MDPC model was reduced to about 5%. Therefore, the MDPC model is in good agreement with the experimental results of Castro (2001). For MC and DP constitutive models, where the behavior of the soil is linearly elastic up to the yield stress level and then becomes completely plastic, the lowest simulation accuracies were obtained due to the lack of hardening definition, compared with the experimental data of Castro (2001). In other words, with increasing confining stress, the behavior of sand tends to harden, and the ability of the MDPC model, which has a hardening function based on volumetric plastic strain, has increased in simulating the behavior of Nevada sand. At confining stresses less than 160 kPa, the maximum deviatoric stresses obtained from MC and DP models had an error of about 1.5% with the predicted values for Arulmoli et al. (based on a stress path of 3:1 in the p' - q' space). This error for the MDPC model was increased to about 7%. In other words, at high confining stresses MDPC model and under low confining stresses, MC and DP models showed the highest simulation accuracy. Also, by increasing the confining pressure, the MC model implemented in the Abaqus overestimates the deviatoric stress of sand. A similar result was obtained by Jarast and Ghayoomi (2018) for saturated Sydney sand at confining stresses of 50 and 100 kPa [46]. The α parameter can be reduced in Abaqus to enhance the accuracy of the MDPC model for low confining stresses. The maximum deviatoric stress of the soil is affected by the α parameter. In

other words, decreasing the α value increases the maximum deviatoric stress of the soil. Consequently, according to Fig. 13 (b), the results of the MDPC model will be consistent with the MC and DP models. According to Shin and Kim (2015), in numerical analysis using the MDPC model, setting α as small as possible is desirable unless the simulation solution does not converge. This parameter for Ottawa sand has been considered 0.01 and 0.05 in the literature [9,11]. The value of α was set to 0.05 for Nevada sand in the present study. Therefore, smaller values of maximum deviatoric stress in the MDPC model compared with those of the MC and DP models are due to the transition surface parameter. It is reminded that α has been introduced to the MDPC model only for numerical stability (convergence of the numerical solution). Therefore, it is not a material constant (Shin and Kim, 2015) [25]. Based on the results, α can be set to 0.01 for confining stresses less than 160 kPa, otherwise to 0.05 (e.g., greater than 390 kPa).

8- Summary and conclusions

During dynamic loading (such as blast loading), the plastic hardening of volume should be considered in the numerical simulation of sandy soils. This type of hardening can be simulated using the cap model in Abaqus. During hydrostatic loading, soils undergo plastic deformation, which may not necessarily lead to failure. Therefore, materials can experience hardening behavior in the cap model if hydrostatic pressure increases. This plastic hardening of volume is the advantage of the cap model (MDPC) over other linear elastic-perfectly plastic models (e.g., MC and DP). In the simulations of geotechnical problems, properly using constitutive models (such as the cap model) requires accurate calibration of model parameters. In the present study, cap parameters of the MDPC model (i.e., hydrostatic compression curve and cap eccentricity) were determined based on the results of laboratory data for Nevada sand at a relative density of 40%. Comparison of cap model results with those measured and computed from MC and DP models indicate proper calibration of hardening parameters for Nevada sand. The results obtained from the present study can be categorized as follows:

1- Under high confining stress (e.g., 390 kPa) MDPC model and under low confining stress (less than 160 kPa), MC and DP models had the highest simulation accuracies in predicting the ultimate deviatoric stress. In other words, with the increase of confining pressure, the behavior of Nevada sand has tended to harden, and the ability of the MDPC model, which has a hardening function based on volumetric plastic strain, has increased in simulating the behavior of Nevada sand.

2- It is desirable to set α as small as possible to improve the accuracy of the MDPC model for low confining stresses. The ultimate strength of the soil in the MDPC model is influenced by the α parameter so that the decrease in α value increases the maximum deviatoric stress. It should be mentioned that the recommended range for α is between 0.01 and 0.05. The parameter α in the MDPC model is only for convergence of the numerical solution and is not a material

constant. According to the results, it is recommended that for low confining stresses $\alpha = 0.01$ (e.g., less than 160 kPa) and for high confining stresses $\alpha = 0.05$ (e.g., greater than 390 kPa).

3- The cap eccentricity parameter (R) does not affect the value of the maximum deviatoric stress of the soil. It is recommended from the present study that the R-value be determined based on volumetric strain corresponding to the peak deviatoric stress of sand. This procedure causes the simulation results to be consistent with the experimental data. Cap eccentricity, R, is highly dependent on the plastic strain. Therefore, the accurate estimation of the R requires choosing the appropriate hydrostatic compression model. In the present study, the best hydrostatic compression model, which appropriately predicted the volumetric strain values under different hydrostatic stresses, has been proposed for Nevada sand based on experimental data.

References

- [1] A. Abdollahipour, M. Fatehi Marji, A. Yarahmadi Bafghi, J. Gholamnejad, A complete formulation of an indirect boundary element method for poroelastic rocks, *Computers and Geotechnics*, 74 (2016) 15–25.
- [2] H. Haeri, V. Sarfarazi, Z. Zhu, M. Fatehi Marji, A. Masoumi, Investigation of shear behavior of soil-concrete interface, *Smart Structures and Systems*, 23 (1) (2019) 81–90.
- [3] H. Haeri, V. Sarfarazi, P. Ebneabbasi, A. Nazari maram, A. Shahbazian, M. Fatehi Marji, A.R. Mohamadi, XFEM and experimental simulation of failure mechanism of non-persistent joints in mortar under compression, *Construction and Building Materials*, 236 (2020) 117500.
- [4] W.F. Chen, G.Y. Baladi, *Soil Plasticity: Theory and Implementation*, (1985) Elsevier Science, Amsterdam, Netherlands.
- [5] D.M. Potts, L. Zdravković, *Finite Element Analysis in Geotechnical Engineering: Theory, Volume 1*, (1999) Thomas Telford Ltd, London, United Kingdom.
- [6] S.W. Sloan, J.R. Booker, Removal of Singularities in Tresca and Mohr-Coulomb Yield Functions, *Communications in Applied Numerical Methods*, 2 (2) (1986) 173–179.
- [7] M.M. Nujid, Numerical simulation of strip footing on sand for bearing capacity analyses, *AIP Conference Proceedings*, 2020 (1) (2018) 020004.
- [8] I.S. Sandler, Review of the development of Cap Models for geomaterials, *Shock and Vibration*, 12 (1 SPEC. ISS.) (2005) 67–71.
- [9] S. Helwany, *Applied Soil Mechanics: With ABAQUS Applications*, (2007) John Wiley & Sons.
- [10] Hibbitt, Karlsson, Sorensen, *ABAQUS/Explicit User's Manual*, Hibbitt, (2000) Karlsson & Sorensen, Inc.
- [11] H. Liu, Dynamic analysis of subway structures under blast loading, *Geotechnical and Geological Engineering*, 27 (6) (2009) 699–711.

- [12] K.Z.Z. Lee, N.Y. Chang, H.Y. Ko, Numerical simulation of geosynthetic-reinforced soil walls under seismic shaking, *Geotextiles and Geomembranes*, 28 (4) (2010) 317–334.
- [13] A.T. Alisawi, P.E.F. Collins, K.A. Cashell, Nonlinear numerical simulation of physical shaking table test, using three different soil constitutive models, *Soil Dynamics and Earthquake Engineering*, 143 (2021) 106617.
- [14] V.A. Hernández-Hernández, D.R. Joya-Cárdenas, L.N. Equihua-Anguiano, J.C. Leal-Vaca, J.A. Diosdado-De la Peña, L. Pérez-Moreno, N. Saldaña-Robles, A. Saldaña-Robles, Experimental and numerical analysis of triaxial compression test for a clay soil, *Chilean Journal of Agricultural Research*, 81 (3) (2021) 357–367.
- [15] S. Bhowmick, Finite Element Modeling of Consolidated Undrained Test of Clay, Technical Report, Memorial university (2021).
- [16] M. Calvello, R.J. Finno, Selecting parameters to optimize in model calibration by inverse analysis, *Computers and Geotechnics*, 31 (5) (2004) 411–425.
- [17] K. Arulmoli, K. K. Muraleetharan, M. M. Hossain, L. S. Fruth, VELACS (Verification of Liquefaction Analyses by Centrifuge Studies) Laboratory Testing Program: Soil Data Report, Washington, (1992).
- [18] R. Popescu, J.H. Prevost, Centrifuge validation of a numerical model for dynamic soil liquefaction, *Soil Dynamics and Earthquake Engineering*, 12 (2) (1993) 73–90.
- [19] M.D. Bolton, The strength and dilatancy of sands, *Geotechnique*, 36 (1) (1986) 65–78.
- [20] T. Schanz, P.A. Vermeer, Angles of friction and dilatancy of sand, *Geotechnique*, 46 (1) (1996) 145–151.
- [21] G. Castro, Redistribution research, Memorandum to Void Redistribution Research Team by GEI Consultants, University of California, Davis, CA, (2001).
- [22] R. Kamai, R.W. Boulanger, Simulations of a Centrifuge Test with Lateral Spreading and Void Redistribution Effects, *Journal of Geotechnical and Geoenvironmental Engineering*, 139 (8) (2013) 1250–1261.
- [23] ABAQUS INC., Analysis of Geotechnical Problems with ABAQUS, (2003).
- [24] H. Shin, J. B. Kim, S. J. Kim, K. Y. Rhee, A simulation-based determination of cap parameters of the modified Drucker-Prager cap model by considering specimen barreling during conventional triaxial testing, *Computational Materials Science*, 100 (PA) (2015) 31–38.
- [25] H. Shin, J.B. Kim, Physical interpretations for cap parameters of the modified Drucker-Prager cap model in relation to the deviator stress curve of a particulate compact in conventional triaxial testing, *Powder Technology*, 280 (2015) 94–102.
- [26] C.S. Desai, H.J. Siriwardane, Constitutive Laws for Engineering Materials, with Emphasis on Geologic Materials, (1984) Prentice-Hall, Inc, New Jersey, United States of America.
- [27] S. Dolarevic, A. Ibrahimbegovic, A modified three-surface elasto-plastic cap model and its numerical implementation, *Computers and Structures*, 85 (7–8) (2007) 419–430.
- [28] L. H. Han, J. A. Elliott, A. C. Bentham, A. Mills, G. E. Amidon, B. C. Hancock, A modified Drucker-Prager Cap model for die compaction simulation of pharmaceutical powders, *International Journal of Solids and Structures*, 45 (10) (2008) 3088–3106.
- [29] Dassault Systèmes, Abaqus 6.14 Example problems guide Volume II: other applications and analyses, Abaqus 6.14 Documentation, (2014).
- [30] G. Oettl, R.F. Stark, G. Hofstetter, A comparison of elastic-plastic soil models for 2D FE analyses of tunnelling, *Computers and Geotechnics*, 23 (1–2) (1998) 19–38.
- [31] C.R.I. Clayton, M.B. Hababa, N.E. Simons, Dynamic penetration resistance and the prediction of the compressibility of a fine-grained sand—a laboratory study, *Geotechnique*, 35 (1) (1985) 19–31.
- [32] M. J. Lee, S. K. Choi, M. T. Kim, W. Lee, Effect of stress history on CPT and DMT results in sand, *Engineering Geology*, 117 (3–4) (2011) 259–265.
- [33] M. Zhang, Y. Yao, H. Pei, J. Zheng, A new isotropic hardening constitutive model based on reference compression curve, *Computers and Geotechnics*, 138 (2021) 104337.
- [34] [34] J.M. Pestana, A.J. Whittle, Compression model for cohesionless soils, *Geotechnique*, 45 (4) (1995) 611–631.
- [35] B.S. Qubain, V.N. Kaliakin, J.P. Martin, Variable Bulk Modulus Constitutive Model for Sand, *Journal of Geotechnical and Geoenvironmental Engineering*, 129 (2) (2003) 158–162.
- [36] S.S. Park, P.M. Byrne, Stress densification and its evaluation, *Canadian Geotechnical Journal*, 41 (1) (2004) 181–186.
- [37] J. Vallejos, Hydrostatic compression model for sandy soils, *Canadian Geotechnical Journal*, 45 (8) (2008) 1169–1179.
- [38] B. Zeleke, Simulation of Pile Load Test Using Finite Element Method, Master’s thesis, University of Addis Ababa, Department of Civil and Environmental Engineering, (2015).
- [39] E. Susila, R.D. Hryciw, Large displacement FEM modelling of the cone penetration test (CPT) in normally consolidated sand, *International Journal for Numerical and Analytical Methods in Geomechanics*, 27 (7) (2003) 585–602.
- [40] S. Alizadeh Sabet, Application of a Cosserat Continuum Model to Non-associated Plasticity, Ph.D. Dissertation, Department of Civil and Structural Engineering,

- University of Sheffield, (2020).
- [41] Dassault Systèmes, Abaqus Version 6.14, (2014).
- [42] S.S. Nagula, R.G. Robinson, J.M. Krishnan, Mechanical Characterization of Pavement Granular Materials Using Hardening Soil Model, *International Journal of Geomechanics*, 18 (12) (2018) 04018157.
- [43] M.M. Eslami, D. Pradel, S.J. Brandenberg, Experimental mapping of elastoplastic surfaces for sand using undrained perturbations, *Soils and Foundations*, 58 (1) (2018) 160–171.
- [44] R. Kulasingam, E. J. Malvick, R. W. Boulanger, B. L. Kutter, Strength Loss and Localization at Silt Interlayers in Slopes of Liquefied Sand, *Journal of Geotechnical and Geoenvironmental Engineering*, 130 (11) (2004) 1192–1202.
- [45] R. A. Jaeger, J. T. DeJong, R. W. Boulanger, I. P. Maki, Effects of state parameter, fines content, and overburden stress on CPT resistance in silty sands, 3rd International Symposium on Cone Penetration Testing, (2014) Las Vegas, Nevada, USA.
- [46] P. Jarast, M. Ghayoomi, Numerical Modeling of Cone Penetration Test in Unsaturated Sand inside a Calibration Chamber, *International Journal of Geomechanics*, 18 (2) (2018) 04017148.

HOW TO CITE THIS ARTICLE

N. Hasanpouri Notash, R. Dabiri, M. Hajjalilue Bonab, L. Khodadadi, F. Behrouz Sarand, A finite element modeling of drained triaxial test on loose sand using different constitutive models, AUT J. Civil Eng., 6(3) (2022) 339-358.

DOI: [10.22060/ajce.2023.22031.5817](https://doi.org/10.22060/ajce.2023.22031.5817)



